sustainability

MDPI

Article

Sustainable Design for CFS Structures: Experimental Data and Numerical Models of Hinged Connections

George Taranu [1,*], Vasile-Mircea Venghiac [1], Ioana Olteanu-Dontov [1], Ancuta Rotaru [2] and Ionut-Ovidiu Toma [1]

[1] Department of Structural Mechanics, Faculty of Civil Engineering and Building Services, Technical University Gheorghe Asachi of Iasi, 700050 Iasi, Romania; vasile-mircea.venghiac@academic.tuiasi.ro (V.-M.V.); ioana.olteanu-dontov@academic.tuiasi.ro (I.O.-D.); ionut.ovidiu.toma@tuiasi.ro (I.-O.T.)

[2] Department of Transportation Infrastructure and Foundations, Faculty of Civil Engineering and Building Services, Technical University Gheorghe Asachi of Iasi, 700050 Iasi, Romania; ancuta.rotaru@academic.tuiasi.ro

* Correspondence: george.taranu@academic.tuiasi.ro; Tel.: +40-232-70-14-55

Abstract: Cold-formed steel structures represent a suitable alternative to classical, by now, structural solutions considering the recycling/reuse tendency worldwide as part of the circular economy paradigm. The paper presents a new design approach for CFS profile joints to accurately predict their realistic behavior, based on experimental and numerical investigation of two types of connectors frequently used in the construction industry for manufacturing joints made of CFS profiles: steel-steel pop-rivets (SSPR) and self-tapping screws (STS). The experiments carried out in the case of T-joints subjected to tensile forces tested both solutions. Another significant parameter of the research was the thickness of the steel sheet used to make the CFS profiles. A number of 20 specimens of T-joints made of Cold-Formed Steel (CFS) profiles in total were tested. These consist of five specimens for each of two types of steel sheet thicknesses. The results are relevant for designers because they provide relevant data concerning the limited axial rigidity of T-joints, which are an important instrument in numerical models for achieving the optimum design of the structural system in terms of strength and overall rigidity. Experimental tests calibrate the numerical model that accounts for the axial stiffness of the hinged joints between the CFS profiles. The main parameters of the research are the thickness of the steel sheet and the connector type. The calibrated numerical model used in a case study highlights the advantages of the new approach compared to the classical design procedure based on a conventional hinged connection. Based on the results, the conclusion is that, besides the geometry of the joint and the connector type, the joint stiffness plays a crucial role in the overall behavior of the structural system and should be accounted for in the design process.

Keywords: cold-formed steel profiles; connector; T-joint; axial stiffness; numerical model

check for updates

Citation: Taranu, G.; Venghiac, V.-M.; Olteanu-Dontov, I.; Rotaru, A.; Toma, I.-O. Sustainable Design for CFS Structures: Experimental Data and Numerical Models of Hinged Connections. *Sustainability* **2022**, *14*, 7813. https://doi.org/10.3390/su14137813

Academic Editor: Elena Mele

Received: 30 May 2022
Accepted: 24 June 2022
Published: 27 June 2022

Publisher's Note: MDPI stays neutral with regard to jurisdictional claims in published maps and institutional affiliations.

Copyright: © 2022 by the authors. Licensee MDPI, Basel, Switzerland. This article is an open access article distributed under the terms and conditions of the Creative Commons Attribution (CC BY) license (https://creativecommons.org/licenses/by/4.0/).

1. Introduction

In a constantly changing society with increasing needs and problems, identifying appropriate material and structural solutions for a sustainable design remains of great interest. Cold-formed steel (CFS) profile structures may represent a solution for this new challenge of achieving a sustainable design process. There are already over 100 years of experience in using CFS [1], but intensive research has been carried out only in the last 50 years [2–5], while in the last 30 years it has begun to increase even more [6–8]. Some of that research focused on profile section or structural systems and others on the connection types between profiles under different type of loadings. The use of CFS structures has seen an increasing interest all over the world from Europe in Italy [9–11], Romania [12–15], Turkey [16], UK [17–19], USA [20–22] or Asia [23–28]. CFS structures may tick some of the requirements in terms of sustainability, such as efficiency ratio (strength vs. consumed material quantity, which allows for an assessment by the proportion between

the strength of a structural element and the mass). According to the Steel Framing Industry Association [29], section C profiles have the highest efficiency ratio among construction products. Bending the thin steel sheets obtains a section with stiffness able to undergo various stresses, in which the kinks themselves represent areas of increased stiffness. On the other hand, CFS profiles present stability over time since they do not bend unless excessive loads are applied, do not crack and can have a lifespan of tens or hundreds of years. Adequate insulation significantly avoids and reduces the risk of subsequent repairs or frequent maintenance checks.

When it comes to the new circular economy paradigm, one of the features that place this product in a top position is the possibility to recycle and reuse the steel into other similar products for several cycles. In the last ten years, the responsibility (urge) of designing and carrying out sustainable constructions to preserve and improve the environment has entered the public consciousness [30].

Flexibility in space repartitioning can be made according to the owner's requirements. This feature is available for constructions with interior walls of CFS profiles that can be modified concerning their position and size during the life cycle of the building, according to the needs. The possibility to mount and dismantle these profiles while using appropriate joints is an advantage because it is no longer necessary to rebuild the covered space completely; it can be converted easily according to architectural needs and without additional structural material consumption.

Green buildings and specific standards according to the Leadership in Energy and Environmental Design (LEED) National Green Building Standard (ICC-700) include the qualities of this material (steel) in the list of those certificated for green buildings because of the ability to reuse and recycle CFS profiles [30] according to architectural needs and without additional material consumption.

Understanding and adopting sustainable construction solutions also means cost-effective results. Energy-saving for steel construction profiles, including costs for material production, saving water and the labor costs can lead to efficient and economically attractive buildings.

CFS thin sheets can be transformed in various complex profile section shapes such as "C", "U", "Z", "∑" and others. The main advantage of structures with steel profiles is the degree of prefabrication of the parts. In particular, "C" section has the advantage of positioning the connected parts in joints with enough space for access to mount with different types of connectors. Due to transport and assembly conditions, the pieces can be connected in the factory or on-site. The joints between the resulting compounds can often fulfil constructive requirements only (without any specific bearing function), but there are cases when they also have a structural role and must be able to properly transmit forces between the elements or ensure sufficient global stiffness to abide by the code requirements [31,32]. The CFS profiles can be mounted in different structural system combinations such as frames, lattice systems, rigid structural panels or combinations of the above. Depending on the dimensions of the covered space and the considered structural approach, various research studies investigate the connection types of joints. The most common connections are made with rivets, self-drilling screws, threaded and nut screws, welds or stampings [33–36]. Many research papers study the nonlinear behavior of both profiles and connectors but address only 3D or 2D finite element modelling and emphasize the profile response [37–41].

The scientific literature presents results on CFS profiles for which the main parameter was the connector type, whether be it rivets, blind-rivets, screws or self-drilling screws. The most used configuration of the investigated joints consisted in two plates of thin steel sheets with different numbers of connectors. The parameters of the considered T-joints presented in the present paper were the thickness of the steel sheet as well as the type of connectors. Numerical and laboratory investigations were conducted in order to calibrate the numerical model and to assess, as accurately as possible, the behavior of the considered joints in direct tensile tests. The optimum combination was selected after careful analysis of

both numerical and experimental investigations. The current research uses C150 × 45 mm profiles to enlarge the possible structural system, as this CFS profile is designed to frame structures, structures with lattice beams and lattice columns reaching an opening of 5.00 m and modulated longitudinally at various distances. Currently available design codes, such as Eurocode 3 [42–45], provide reasonable information on the analytical approach to account for the behavior of elements. Consequently, numerical models based on the analytical approach provided in Eurocode 3 may require further significant calibration to match the experimental programs. For example, considering a hinged lattice beam with infinite axial stiffness, the general rigidity of the truss may be overestimated, and the strength capacity of some of its components may be exceeded due to a redistribution of internal forces.

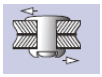
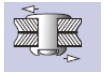
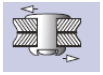
The current study highlights the importance of using force–displacement curves assessed through experiments on the joint types between the profiles of a structural system. Experimental results are comparable to those obtained in other research works available in the scientific literature [46,47].

2. Materials and Methods

2.1. Steel Quality and Connectors

The considered materials are among those available on the market for cold-formed steel profile products. The steel sheets used to form the C profiles have S355 steel grade. The initial purpose of the research was to study the behavior of this type of steel to establish whether these profiles are suitable for load-bearing structural elements. Table 1 presents the steel-steel pop-rivets and self-tapping screws considered for the connections.

Table 1. Materials properties.

Joint part	Material	Strength	
Flange Post C150 × 45 × 10 t = 1.2/1.6 mm	S355 [42]	355 MPa—Yield strength experimental	490 MPa—Maximum strength experimental
Steel-Steel pop-rivets 4.8 × 10 mm [48] 	Zinc coated steel	 2900 N—Shear strength [48]	 3100 N—Tensile strength [48]
Self-tapping screw 5.5 × 22 mm [48] 	Zinc coated steel	 500 MPa—Shear strength [48]	 1000 MPa—Tensile strength [48]

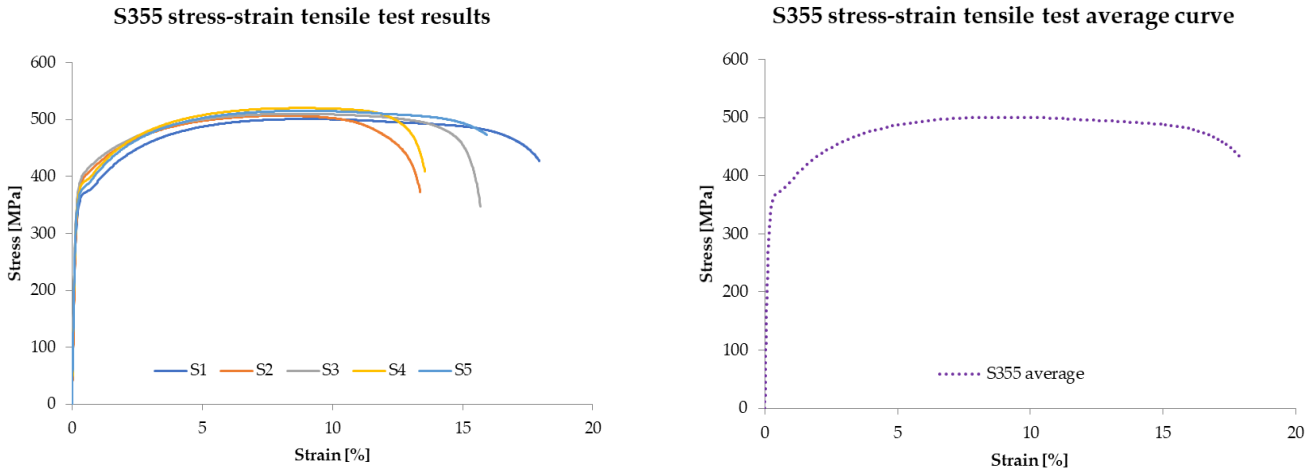
To correctly identify the material and its behavior, experimental tests were carried out according to ISO 6892-1:2019 specifications [23] on samples cut from steel sheet. The steel specimens were cut from the web of the CFS profiles. In the laboratory, five specimens were tested in the ZWICK/ROELL 1000 SP universal test machine. The universal testing machine is hydraulic and has a single central hydraulic drive. The bottom part of the machine is fixed and the upper part can move in a range of 0 to 60 cm. The maximum test speed of the machine is 200 mm/min. The universal testing machine is fully automated and controlled by the TestXpert II v3.5 software. The test speed was based on stress at a rate of 30 MPa/s.

Figure 1 shows the considered specimens extracted from the CFS profiles. The strains were measured using an external extensometer attached by contact to the specimen. Figure 2 shows the stress–strain curves obtained on all the tested samples.



(**a**) (**b**)

Figure 1. Laboratory experimental test on S355 steel sheets: (**a**) samples with extensometer mounted in universal testing machine; (**b**) samples tested.



(**a**) (**b**)

Figure 2. Stress–strain curves for S355 steel sheet in tensile test: (**a**) curves for the 5 specimens; (**b**) average curve.

2.2. Connection's Geometry and Testing Methodology

Figure 3 presents the geometry of the elements making up the T-joint and the geometry of the joint itself. Both interconnected parts have a hole located in the center of the contact area of the C-profile flange where the connector sets in.

The specimens were mounted in the universal testing machine employing steel adaptors, with the primary role being to align the joint with the direction of the applied tensile load. A 10 mm thick welded T-shaped steel adaptor connected the joint to the lower grips of the testing machine. The experiment uses a 300 × 150 × 10 mm steel sheet in the upper part, as shown in Figure 3. 4 M14 screws fastened these adaptor pieces at the upper and lower regions of the T-joint. A constant loading rate of 50 N/s was applied until the failure occurred. The internal transducer of the testing machine recorded the absolute displacements.

The labelling of the tested specimens shown in Figure 3, which depends on the connector type and the thickness of the steel sheet, is explained in detail in Table 2. Two series of specimens operated based on the steel sheet thickness of the CFS profiles. For

each of the two series, two different connector types were considered. Furthermore, each sub-grouping consisted of five specimens for 20 specimens in total. Hence, the specimen labeling had in view the specimens (S), the sample number within the sub-group (1–5), the series type based on steel sheet thickness (A or B) and the type of connector (SSPR or STS).

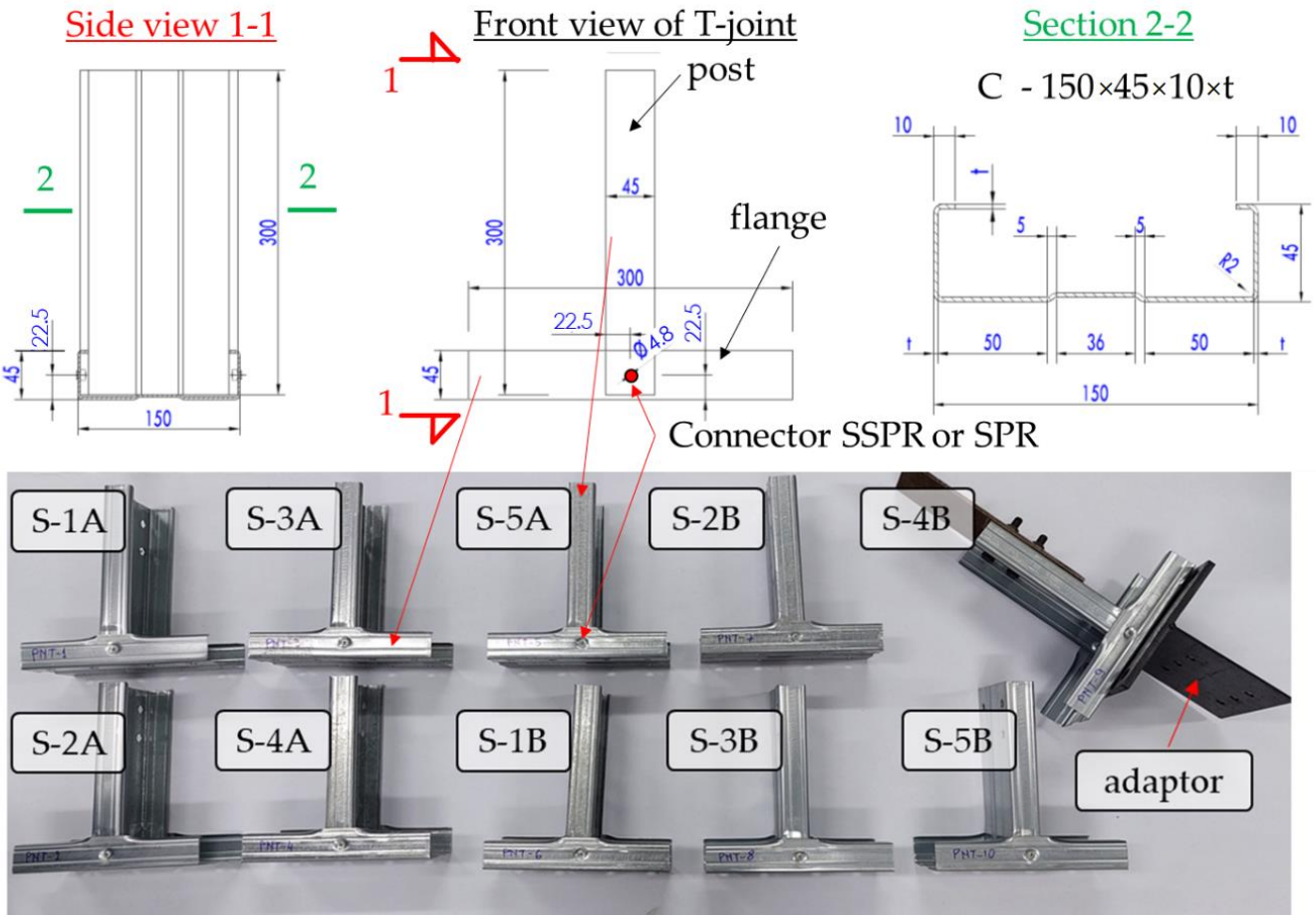


Figure 3. Geometry and dimensions for the tested joints, C-profile characteristics, respectively.

Table 2. Experimental tested specimen label and description.

Specimen		C-Profile Thickness (mm)	Connector
S-1A SSPR	S-1A STS	A = 1.2	(SSPR) Steel-Steel Pop-Rivet
S-2A SSPR	S-2A STS		
S-3A SSPR	S-3A STS		
S-4A SSPR	S-4A STS		
S-5A SSPR	S-5A STS		
S-1B SSPR	S-1B STS	B = 1.6	(STS) Self-Tapping Screw
S-2B SSPR	S-2B STS		
S-3B SSPR	S-3B STS		
S-4B SSPR	S-4B STS		
S-5B SSPR	S-5B STS		

Figure 4 shows the details of mounting the joint specimens in the Zwick/Roell 1000SP universal testing machine and details of the used connectors.

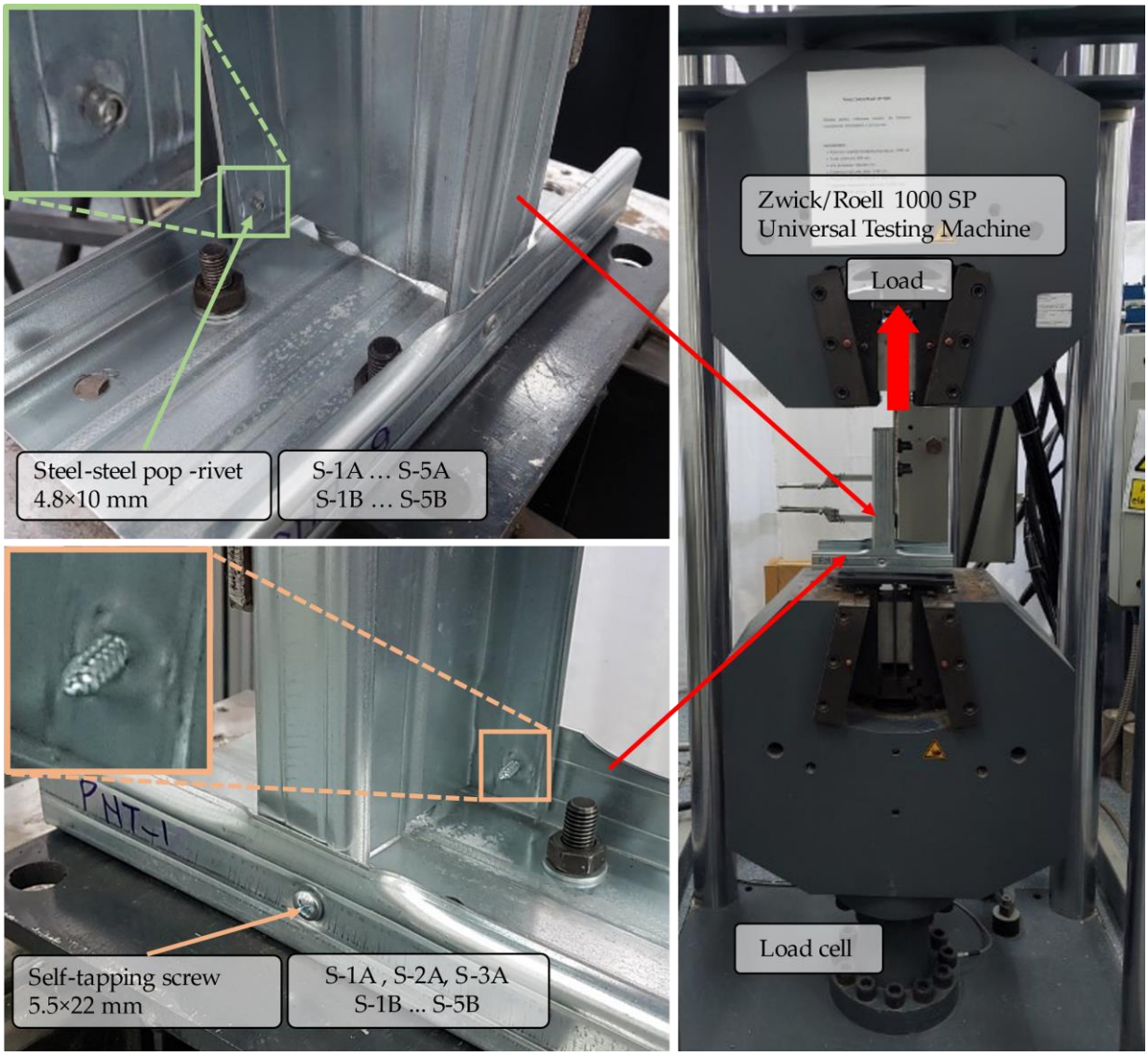


Figure 4. Testing equipment, specimens and connector details.

A 10 T-joint sample set with SSPR connectors was ready during the first stage. After their failure and the investigation of the pre-drilled holes, the elements met together again using self-drilling screws of Ø5.5 × 22 mm. The new joints were tested again with the same test parameters to assess an aspect of the sustainability properties for CFS presented at the beginning, namely their capacity to be reused after a dismantling process. The number of the reuse cycle evaluation and the effect on the residual strength capacity of the elements to be recycled are topics of future research.

3. Experimental Testing Results

3.1. Experimental Results for Connections with Rivets—SSPR

The TestExpert control program recorded and exported the force–displacement curves (P-Δ) for post-processing and analysis. Figure 5 shows the comparative overlapping curves for each of the five distinct situations mentioned in Table 2.

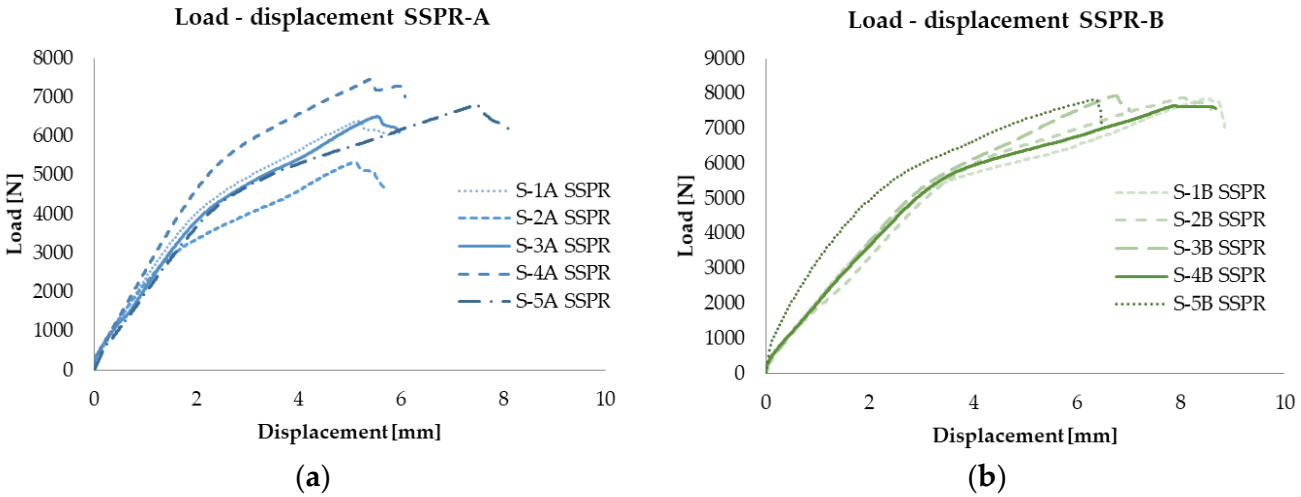


Figure 5. Force–displacement results for (**a**) joint connection type SSPR-A; (**b**) joint connection type SSPR-B.

The graph in Figure 5a shows that the maximum load value for SSPR-A joints reached approximately 7400 N per node only for specimen number 4 and a displacement of 5.4 mm, while all the others were around 6500 N with a 5.5 mm maximum displacement. That shows that in the 1.2 mm steel sheet case, the shearing and crushing of the rivet caused the failure. In the case of the increased thickness, the B series with a 1.6 mm thickness, which used SSPR joints, experienced a complex stress state in the rivets located on the larger contact surface between sheets and rivets, which were crushed, bent and sheared. The maximum recorded value was 7900 N, which was 21% higher than in the case of SSPR-A, at a displacement of 6.40 mm, as shown in Figure 5b.

3.2. Experimental Results for Connections with Screws STS

In the case of the A series with STS connectors, only three results were allowed due to technical causes, as shown in Figure 6a. Thus, a maximum load value of 16,500 N, with a corresponding displacement of 15 mm, was obtained in the case of S-1A STS. Meanwhile, the average peak load value was 15,300 N with a 16.85 mm corresponding displacement. In the case of the B series, Figure 6b, the STS-B samples reached a maximum value of 20,100 N and a corresponding displacement of 19.6 mm for S-3B STS. The average load value for STS-B samplings was 18,500 N, recording a 17.5 mm displacement.

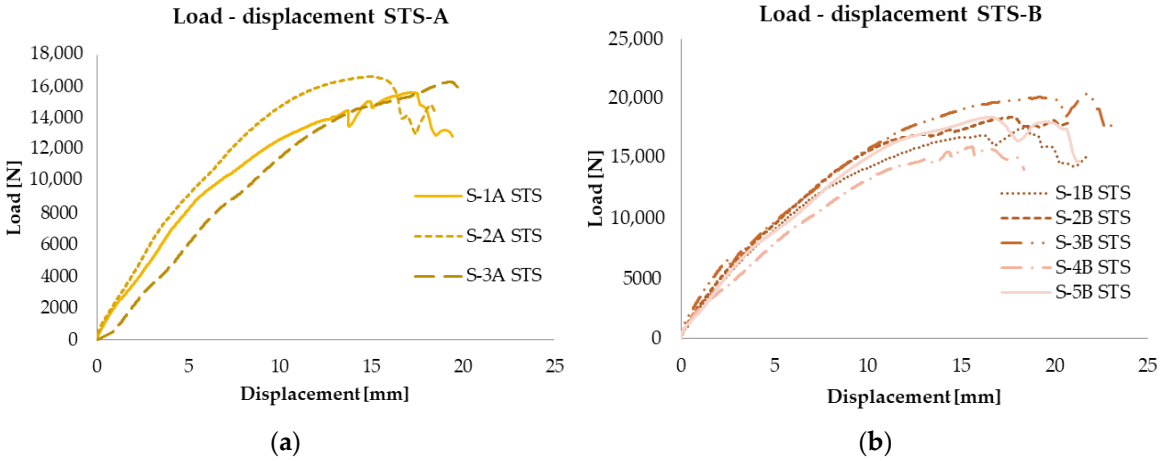


Figure 6. Force–displacement results for (**a**) joint connection STS-A; (**b**) joint connection STS-B.

All average force–displacement curves are compared graphically in Figure 7. The results show that both sheet thickness and connector type influence the behavior and the load-carrying capacity of these joints. Four distinct areas allow identification from the force–displacement curve analysis for the SSPR-A and SSPR-B joints. The four areas indicated on load-displacement SSPR-A average curve in Figure 7 are similar for other types of joints tested.

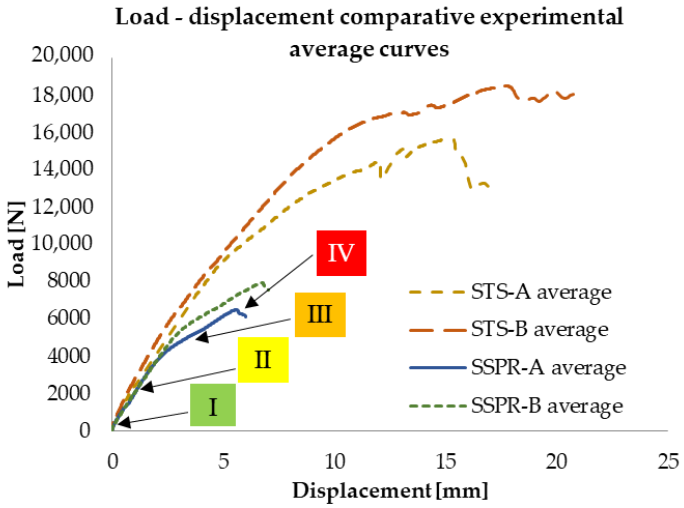


Figure 7. Comparison of the experimentally obtained average force–displacement curves.

According to the stiffness highlighted in Figure 7, the four distinct areas of the joint's behavior consider the stiffness of the connection as follows:

1. In Area I, the initial stiffness attained 2150 N/mm for SSPR-A and 2170 N/mm for SSPR-B. For the screw joints, the initial stiffness reached 2295 N/mm for STS-A and 2360 N/mm for STS-B, respectively. These initial values are about 40% higher than the stiffness in the elastic Area II due to the presence of embedded drawings.
2. Area II, with elastic behavior, is wider compared to the initial one. The average stiffness value was 1520 N/mm for SSPR-A and 1598 N/mm for STS-B.
3. Area III corresponds to the plastic range when the displacements increase more than the loads. The average stiffness was 628 N/mm for SSPR-A and 677 N/mm for STS-B.
4. Area IV represents the failure area when the node can no longer take loads, and the displacements increase until the rivets break or the screws are torn-up due to the shearing of the material around holes.

These stiffness values and the idealized bilinear curves of the node behavior obtained through experiments are the input data for the finite element numerical simulation. Namely, they are in the definition of the nonlinear behavior of hinged joints. Section 4 of the paper summarizes the stiffness values and idealized curves according to the Robot Structural Analysis calculation software requirements [49].

3.3. Failure Modes of the SSPR and STS Connections

Figure 8 shows the failure mechanism of the SSPR-A joint connection with a detail of the rivet status after failure. Small surfaces indicating little worn-out areas on the steel profile are also noticeable between the drawn areas around the holes of the profile. The marked area presence showed increased friction between the elements and an initial stiffness increase of up to 10% from the maximum loading value. The areas with plastic deformations were not visible to the naked eye after the failure of the rivets in the connection area.

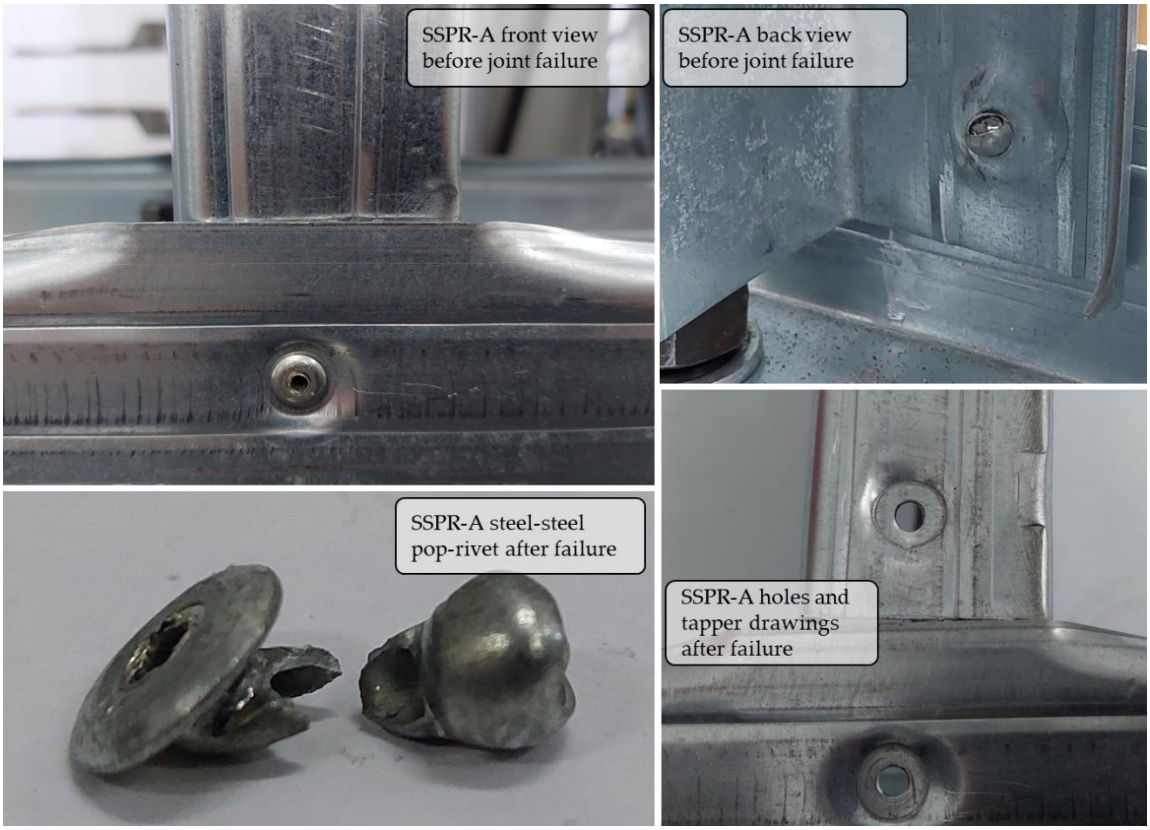


Figure 8. Failure mechanism of steel-steel pop-rivets joints SSPR-A.

Figure 9 presents the failure of an SSPR-B joint and the contact areas between elements, highlighting their post-failure aspect. Slight worn-out surfaces appearing in the lower part of the drawing areas of the strut elements and the upper part of the drawing areas of the horizontal component denoted by 1 in Figure 9 were identified, which means that the friction between the elements during the tests was significant in the first stage. Plastic deformation areas develop to a small extent at the hole level in the strut. The rivets failed due to a combination of bending, crushing and shearing.

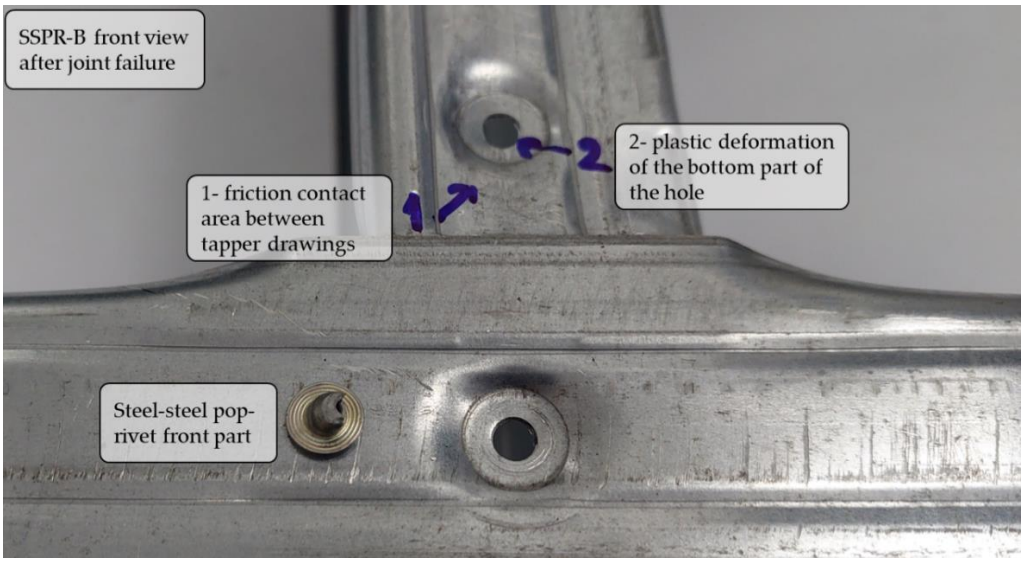


Figure 9. Failure mechanism of steel-steel pop-rivets joints SSPR-B.

Figure 10 shows details of the failure mechanism of a STS-A joint regarding the rotation of screws, the local bending of drawing cups and the plastic deformation of holes. Figure 11 presents a similar failure mechanism observed for the case of STS-B joints. The existence of screws and their thread favored a more ductile behavior, the final failure mechanism being gradual as opposed to the failure mechanism observed for the joints with rivets that failed in a brittle manner.



Figure 10. Failure mechanism of self-tapping screw joints STS-A.



Figure 11. Failure mechanism of self-tapping screw joints STS-B.

4. Numerical Simulation of Joints with 1D Finite Elements

4.1. Input Data

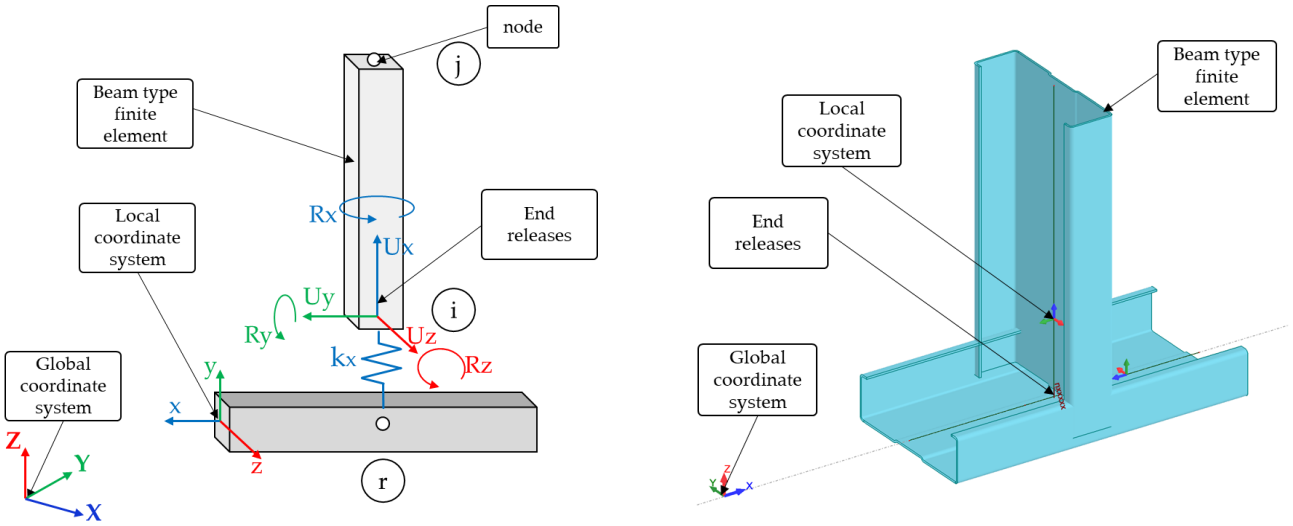
According to Chapter 5, Section 5.1.1 from EN 1993-1-1 [42], the structural model and the simplifying assumptions must reflect, as accurately as possible, the actual behavior of the structures in the limit states and show the factual behavior of the sections, elements, joints and supports. In the Section 5.1.2 of the same norm [42] it is stated that "Generally, the effects of the joint behavior on the distribution of internal force and moment distribution within a structure and the overall deformations of the structure, may not count. However, where such effects are significant, such as for semi-continuous joints, they should be included, EN 1993-1-8" [42,44]. Moreover, the checking procedure of the joint's strength according to EC 3 1-1-3 [26] does not take into account the non-linear behavior of the joints.

Generally, the finite element modelling of structures with bar-type elements considers the hinged connections free to rotation and restrained against translations, respectively, having infinite axial stiffness. In the case of CFS profile structures, how the bond between bars is defined has a considerable influence on results in both static and dynamic responses, sometimes underestimating them. A comparative analysis with 1D finite elements and hinged links observed in three different scenarios the effect of nonlinear behavior on element connection. The material used to model the joints and truss is S355 with modulus

of elasticity E = 210 GPa. The finite elements are beam type and the distance between nodes varies from 100 mm to 300 mm. The modelling of axial rigidity in end releases of the elements is based on next types of behavior:

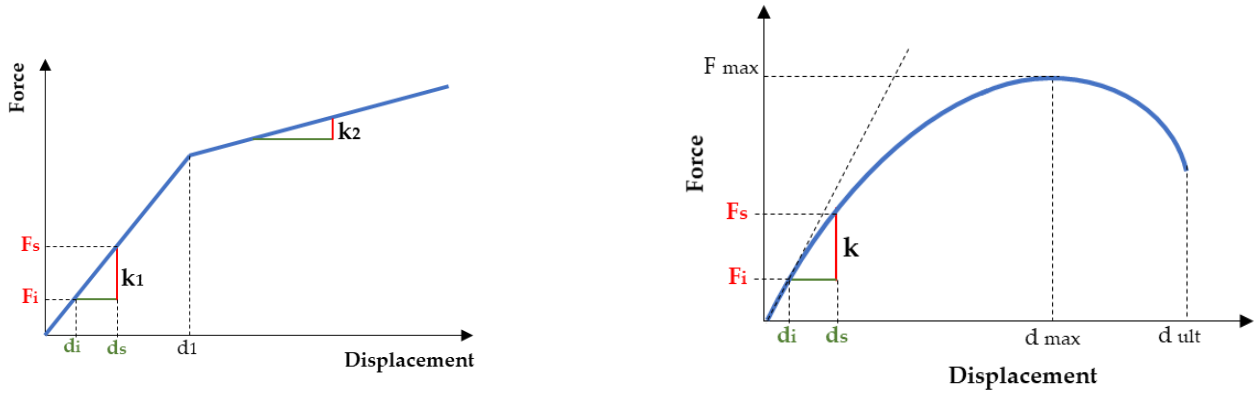
- Linear (conventional);
- Nonlinear, of bilinear type;
- Nonlinear, of parabolic type.

Figure 12a shows the experimentally tested joint, which was analyzed in Robot Structural Analysis software [24], and Figure 12b defines the degrees of freedom in the nodes for the bar-type finite elements. Thus, the experimental results with bilinear (Figure 13a) and polynomial (Figure 13b) behaviors define the axial stiffness kx.



(**a**) (**b**)

Figure 12. Hinged joint with nonlinear behavior (**a**) conceptual sketch for the degree of freedom for the T-joint of beam type elements; (**b**) numerical model geometry.



(**a**) (**b**)

Figure 13. Characteristic curves for the axial stiffness, k_x: (**a**) Idealized bilinear representation; (**b**) Polynomial curve.

The considered relation computing the stiffness is:

$$k = \frac{F_s - F_i}{d_s - d_i} \quad (1)$$

where F_s and F_i represent the limit values of the considered interval, d_s and d_i the displacements corresponding to the forces, according to the curves in Figure 13.

The stiffness values acquired based on the recorded experimental data for each area are summarized in Table 3 and presented graphically in Figure 14. Although the initial axial stiffness is slightly higher, its small influence on the overall behavior of the joint made it neglected. Therefore, $k_x = k_e = k_1 = k$, which is the first value of the axial rigidity in the elastic behavior presented in Figures 13a and 14, respectively, and $k_p = k_2$ mentioned also in Figures 13a and 14, were adopted.

Table 3. Stiffness values with respect to the sheet thickness and the connector type.

Joint Type	Stiffness [N/mm]			F_{max} [N]	d_1 [mm]	d_{ult} [mm]
	k_i	$k_x = k_e = k_1 = k$	$k_p = k_2$			
SSPR-A	2150	1520	628	6150	2.65	5.50
SSPR-B	2170	1560	644	7800	3.20	7.00
STS-A	2295	1575	669	14,500	5.85	12.50
STS-B	2360	1598	677	17,400	8.40	13.20

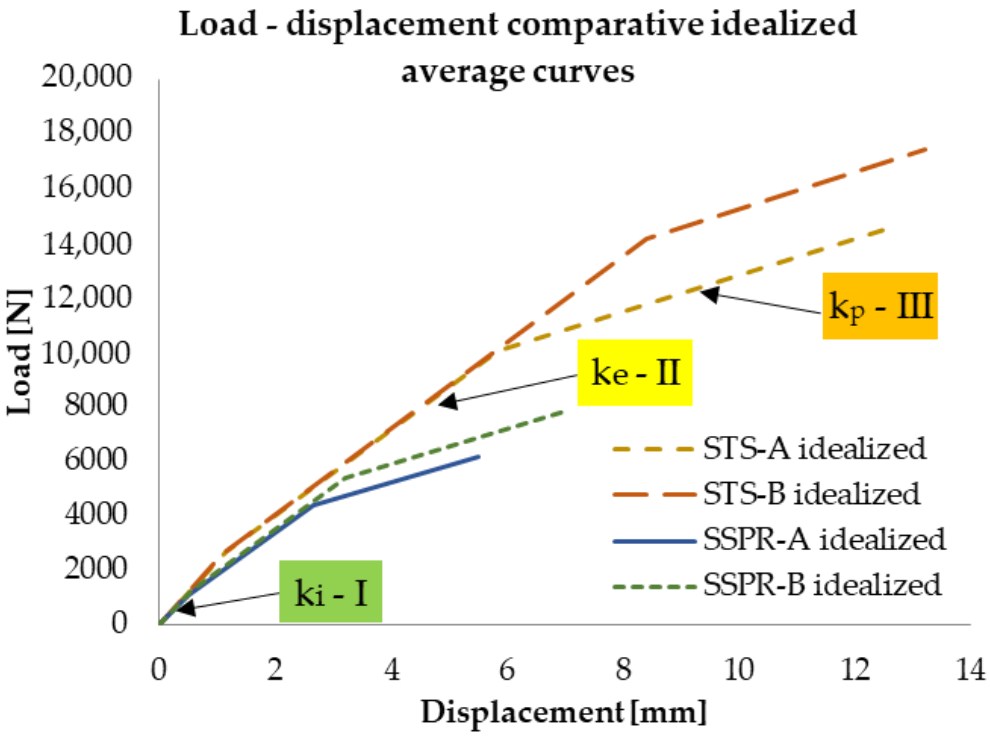
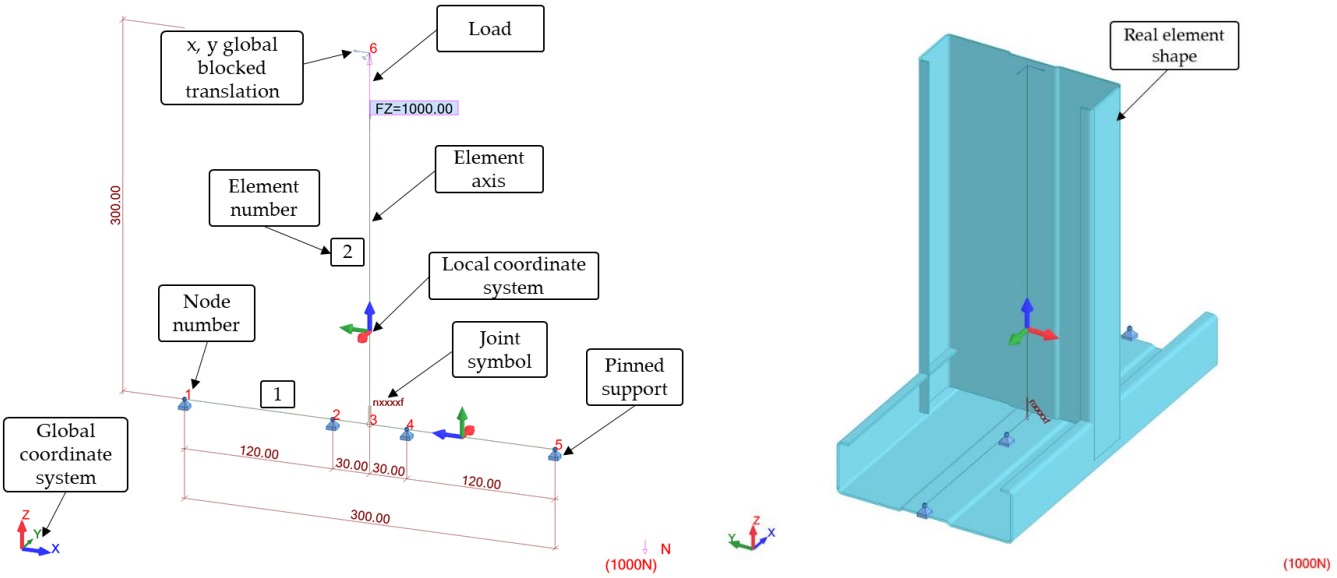


Figure 14. Comparison between the experimental idealized curves.

4.2. Joints Modelling

Figure 15 presents the geometric model for the joint. The flange of the joint was fixed by four pinned supports arranged according to the layout shown in Figure 15a. At the top part, in node 6, the translations in the X and Y directions of the global coordinate system were restrained. The force was applied at node 6 with 1000 N increments from 1 to 10,000 N and with 2000 N step size from 10,000 N to 20,000 N.



(**a**) (**b**)

Figure 15. (**a**) Conceptual diagram of the joint; (**b**) 3D view.

The degrees of freedom for node 3 of element 2, Figure 15a, are shown in Table 4.

Table 4. Considered scenarios for the degrees of freedom at the pin-connection/hinge.

Degree of Freedom (DOF)	Conventional Joint Linear	Nonlinear SSPR-A	Nonlinear SSPR-B	Nonlinear STS-A	Nonlinear STS-B
U_x	blocked	Nonlinear SSPR-A bil/pol	Nonlinear SSPR-B bil/pol	Nonlinear STS-B bil/pol	Nonlinear STS-B bil/pol
U_y	blocked	blocked	blocked	blocked	blocked
U_z	blocked	blocked	blocked	blocked	blocked
R_x	blocked	blocked	blocked	blocked	blocked
R_y	blocked	blocked	blocked	blocked	blocked
R_z	free	free	free	free	free

4.3. Numerical Analysis Results for the Joints

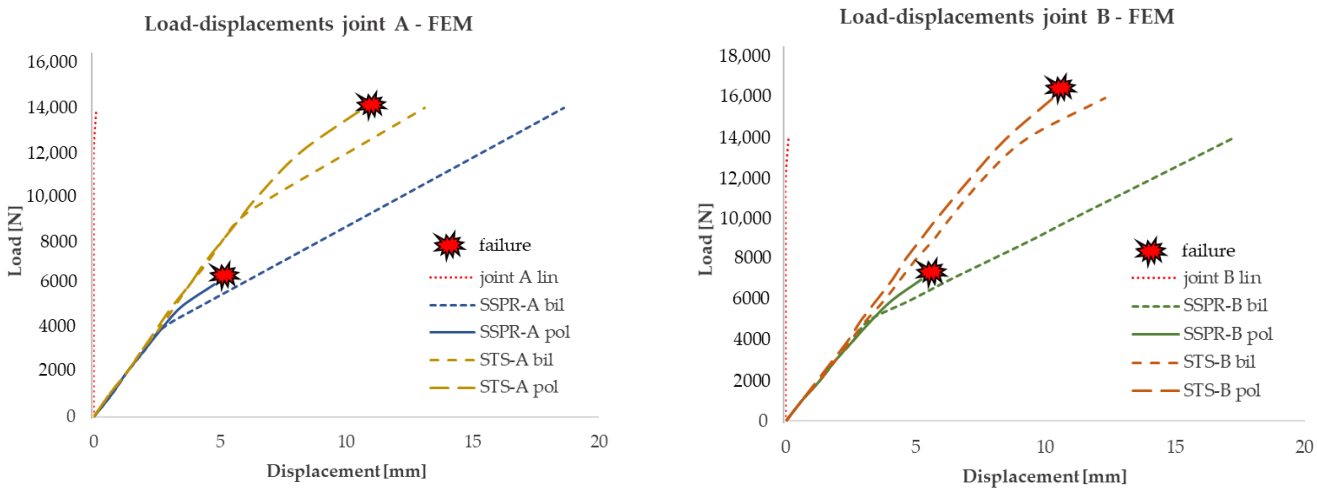
In the case of conventional linear analysis in which the bar 2 was hinged, by applying the increasing force from 0 to 10,000 N the maximum displacement of node 6 was 0.1 mm at a 14,000 N maximum load. In the graphs from Figure 16a,b the comparative curves present the five distinct models:

- Joint A/B lin—the basic model with a hinged joint;
- SSPR-A/B bil—model with bilinear behavior of the axial stiffness of bar 2;
- SSPR-A/B pol—model with polynomial behavior of the axial stiffness of bar 2;
- STS-A/B bil—model with bilinear behavior of the axial stiffness of bar 2;
- STS-A/B pol—model with polynomial behavior of the axial stiffness of bar 2.

In the bilinear model case, SSPR-A bil, when reaching the limit displacement value of 2.7 mm, the observed change in the slope by a faster increase of displacements did not interrupt the convergence. In the STS-A bil case, at a 5.8 mm displacement, the slope of the graph changed. These values coincide with those introduced by the bilinear curves of the axial bond.

In the case of modelling the SSPR-A pol joints with the polynomial function when reaching the 2.7 mm displacement, the stiffness of the node changed until reaching the final displacement of 4.8 mm at a force of 6000 N when the solution became non-convergent.

That represents the failure point marked on the graph with a red star. The situation was similar in the case of STS-A pol, the final displacement being 10.7 mm at 14,000 N.



(**a**) (**b**)

Figure 16. (**a**) Numerical results for joint type A; (**b**) Numerical results for joint type B.

The results for the type B joints shown in Figure 16b are similar to those of the type A, the ultimate displacement, which in the SSPR-B bil case was 2.6 mm and 5.2 mm for SSPR-B pol, representing the main differences between them. By increasing the thickness of the sheet profile in the case of the model with polynomial function at the same load of 7000 N, the node type B was stiffer than A, with a total displacement smaller by 10%.

For the STS-B bil model, the limit value for the displacement was 9.3 mm at 14,000 N and in the case of STS-B pol, it was a 10.3 mm ultimate displacement corresponding to an applied force of 16,000 N. In the case of the joint type B with polynomial function, the maximum force value was 16,000 N, at which the convergence of the solution stopped.

In Figure 17, a comparison between the curves of the analyzed models, defined through a polynomial curve for the axial stiffness, was performed. These are very similar to those experimentally obtained. The curves are separated based on the profile thickness to simplify the comparison and identify the differences, as seen in Figure 18a for type A and b for type B.

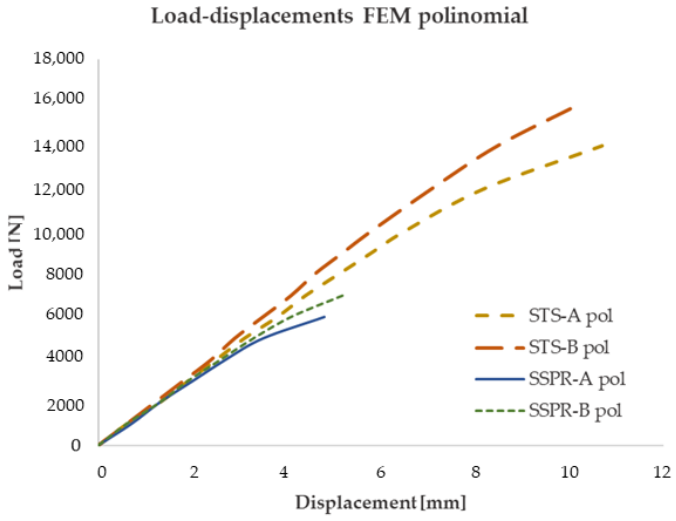
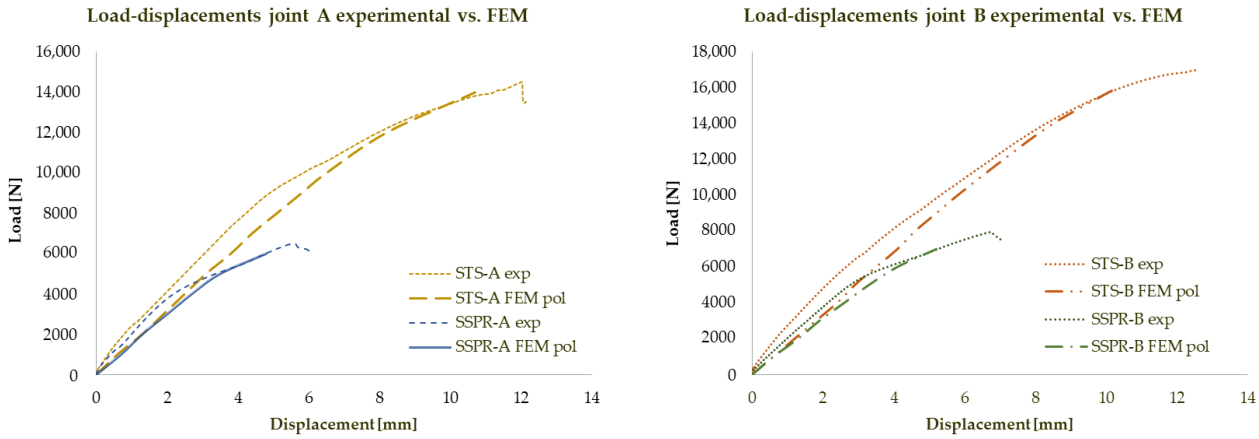


Figure 17. Comparison of the curves from numerical simulation with the polynomial function.



(**a**) (**b**)

Figure 18. (**a**) Comparison of experimental and numerical curves for type A joint; (**b**) Comparison of experimental and numerical curves for type B joint.

The maximum stress in the joint type A identified in bar 2 at a load value of 6000 N was 20.17 N/mm^2. At a force of 10,000 N, the maximum stress was 33.61 N/mm^2, except for the SSPR-A pol case, which no longer converged after reaching the failure point.

In the case of the joint type B, the maximum stress obtained in element 2 was 15.12 N/mm^2 at a load of 6000 N, and at 10,000 N, the maximum stress was 25.21 N/mm^2 except for SPRB-pol, which no longer converged.

5. Case Study on a 2D Truss Beam

5.1. Structural Analysis Assumptions

The proposed comparative analysis of a 2D truss beam highlighted the influence of the authentic behavior of joints connected with self-tapping screws. The truss modeling assumes two approaches: conventional with linear hinged joints and nonlinear with joints defined using the STS-B pol—the polynomial model.

The beam shown in Figure 19 has an opening of 5000 mm and a height of 500 mm. It was simply supported at joints 1 and 17 and restrained against translations in the global y-direction for all the joints positioned in the top chord. It was divided into eight panels 625 mm in length. The diagonal positions were eccentrical concerning the nodes of the struts with an eccentricity of 50 mm on the flange. The forces were applied concentrated at the nodes at the top chord. The load intensity varied from 250 N to 3500 N for ten loading scenarios, as shown in Table 5.

Table 5. Loading scenarios.

Case	Nodes	Load F_z (N)
1	18, 20, 22, 24, 26, 28, 30, 32, 34	−250
2		−500
3		−700
4		−1000
5		−2000
6		−3000
7		−3250
8		−3350
9		−3400
10		−3500

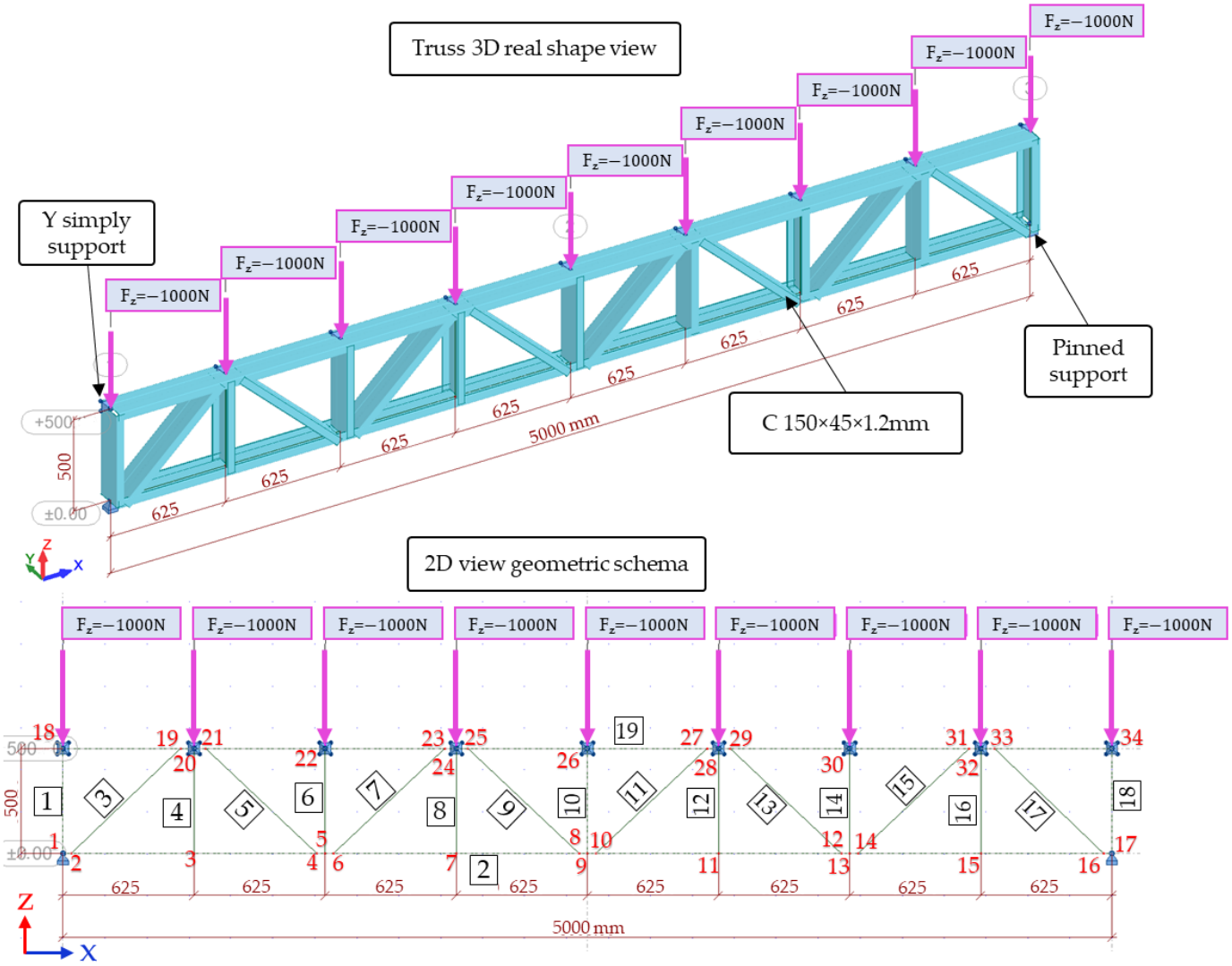


Figure 19. Geometry and static model for the truss structure.

5.2. Results

The monitored results assessed the maximum vertical displacements occurring at joints 9 and 26, located at the mid-span on the bottom and top chords, respectively. Considering the stiffness, the maximum displacement should occur below L/250 = 20 mm which is the maximum allowable displacement according to design codes. That resulted in the case of a load intensity of 700 N on each node. Figure 20 shows the deformed shape of the truss model to the undeformed one in both configurations; that is, conventional hinged nodes and node behavior defined by the polynomial function.

Comparing the maximum displacements shown in Figure 20, the maximum displacement at node 26 was 1.0 mm at a load intensity of 700 N on each node in the model with conventional joints, which means a total beam load of 6.30 kN. In the case of the model with non-linear defined joints, the maximum displacement at the same node was 19.8 mm, representing 99% of the maximum allowable displacement. Accordingly, the difference is almost 20 times the overall stiffness of the truss beam.

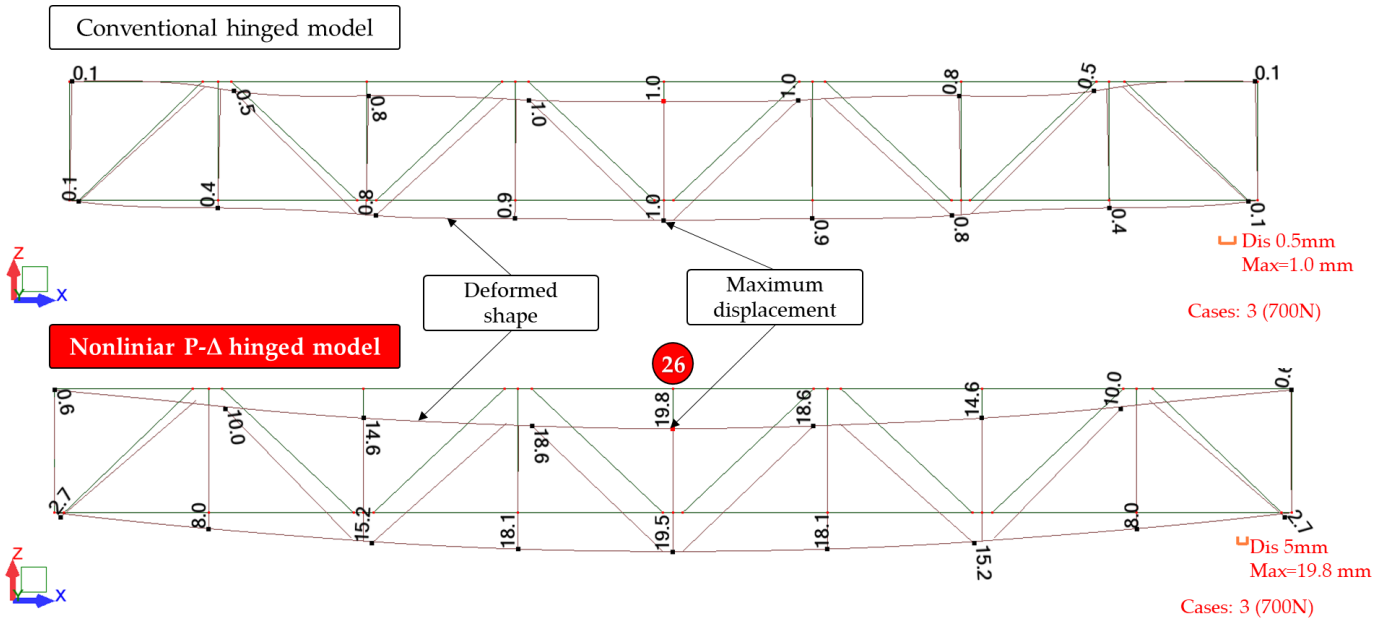


Figure 20. Deformed shape for the truss at a load of 700 N per node considering both case studies.

Figure 21 shows the distribution of the axial forces in the bars of the truss structure considering the same loading case as for the displacement computation (700 N/joint) in both model approaches. The maximum value of axial forces shows a relatively small difference. In the case of the compressed top chord, bar 19, the maximum axial force was 6953 N, 7.5% higher in the conventional hinged model in contrast to the nonlinear model, which had a 6436 N axial force. In the case of the lower chord, bar number 2, the maximum obtained value for the axial force was 2205 N, 8% higher in the conventional model than 2025 N in the nonlinear model. The differences are also inverse in bars 1 and 18, which are more stressed in the nonlinear model, and also in bars with reversed loading states from tension to compression (bars 4 and 16).

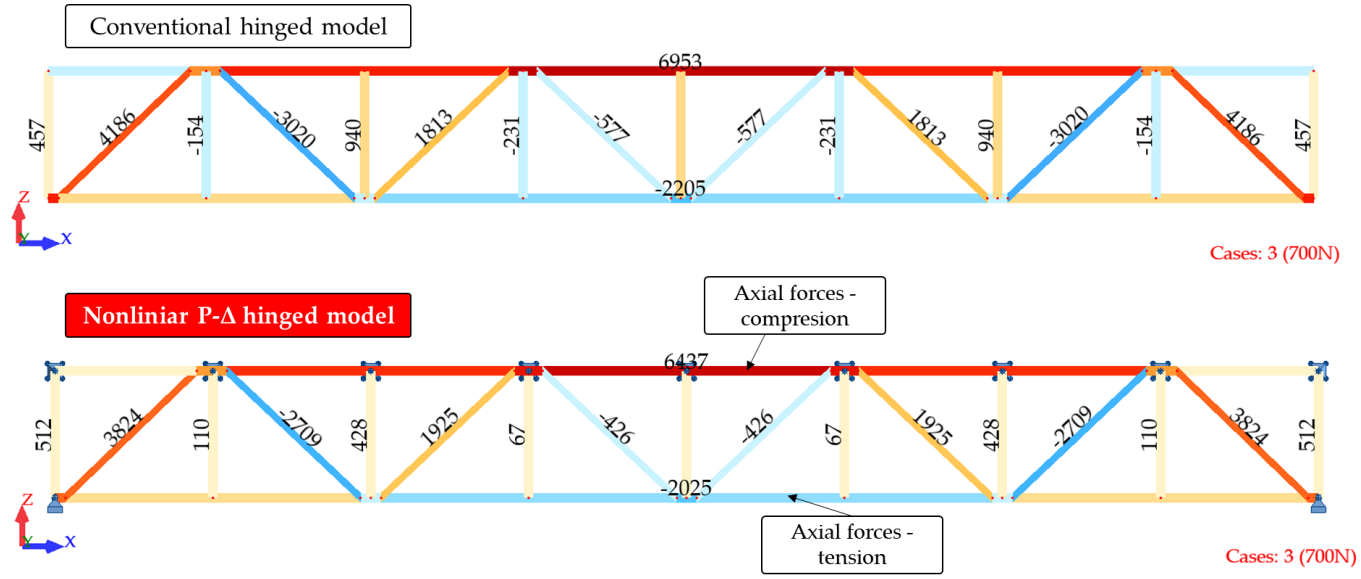


Figure 21. Axial force distribution in loading case 3, considering both case studies.

Analyzing the stress state in the truss bars (Figure 22), they reach the value of 283 N/mm^2 in the conventional model at joints 19 and 33, located on the top chord and belonging to the first and last panels of the truss. For the nonlinear model, the maximum

stress of 343 N/mm^2 occurs at nodes 21 and 31, also located on the top chord but belonging to the second and the last panels of the truss. The total load applied to the truss for both models was 30 kN.

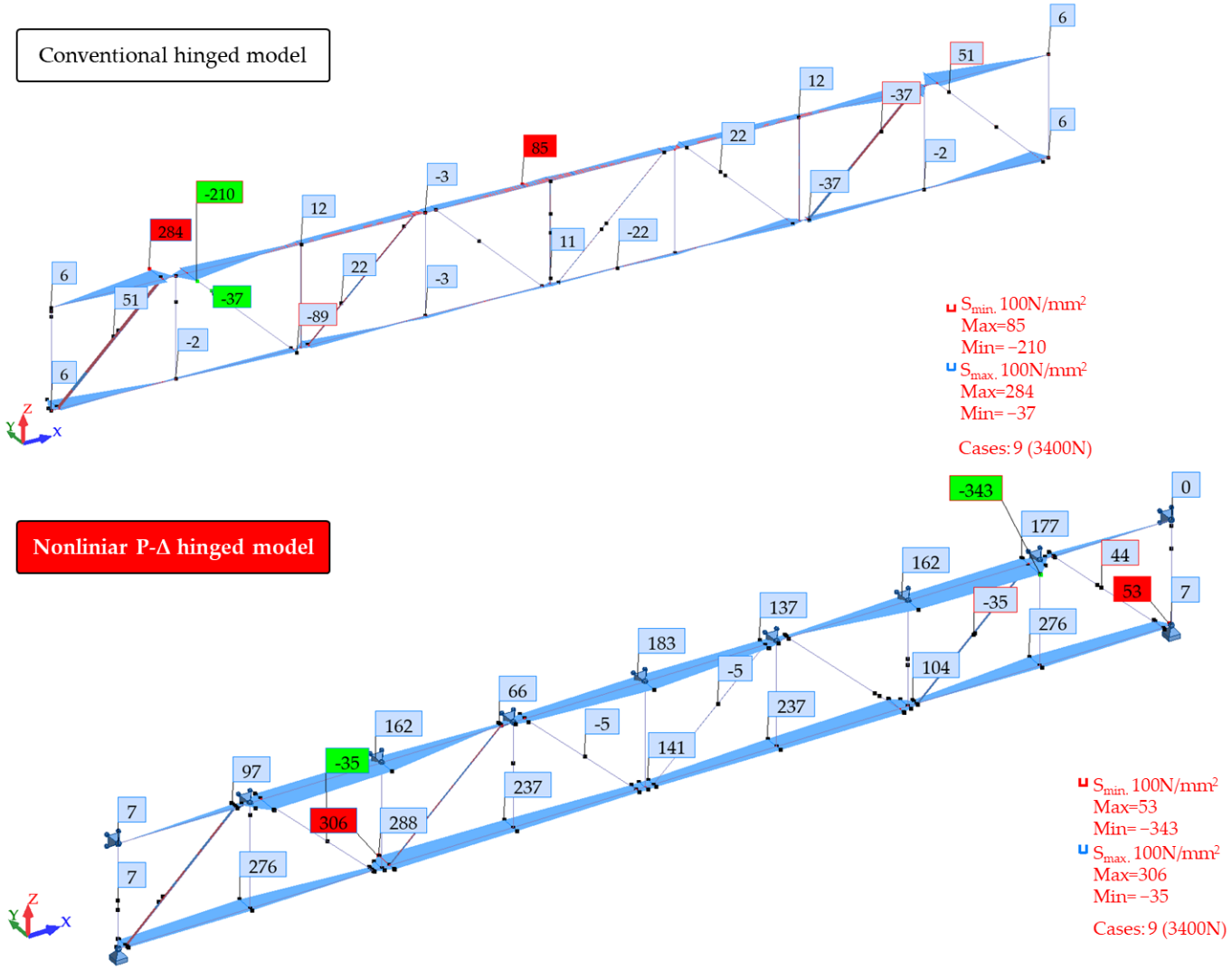


Figure 22. Maximum normal stress distribution.

Figure 23 shows a force–displacement curve computed on the relation between the total loads on the truss as the sum of all the forces per node applied up until the failure of all the non-linearly defined connections occurs. The nonlinear model is much more flexible at a maximum displacement of about 100 mm, reaching a load of around 30 kN. The structure yields; this did not occur in the conventional linear model. Moreover, the maximum displacement of only 5 mm at the same value is significantly reduced.

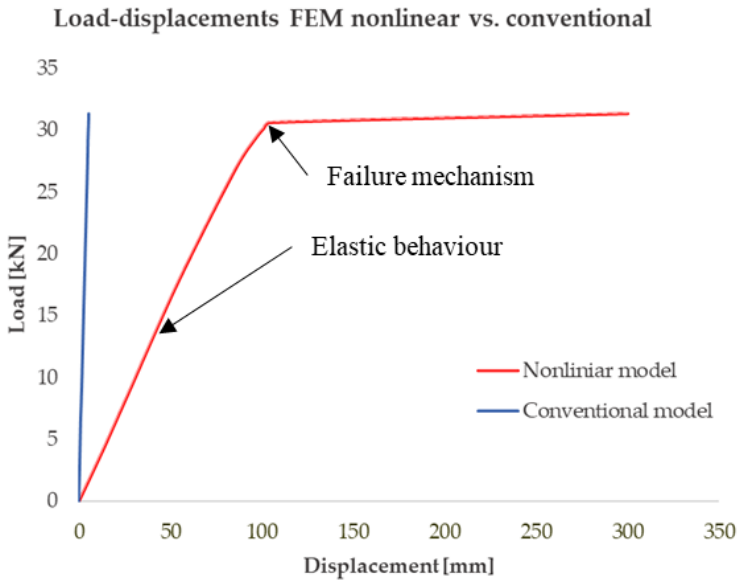


Figure 23. Force–displacement curve for the truss beam.

6. Discussion

The laboratory tests have led to similar results reported in the scientific literature to record force–displacement curves [39] with maximum load from 8 to 30 kN and maximum displacement from 3 to 8 mm. The difference is that the tests were not carried out on the T-joint, just on steel sheets with different patterns and numbers of screws. The use of SSPR and STS connectors in daily practice is the preferred solution by contractors as they are technologically accessible. The STS connectors lead to a higher load-carrying capacity of the joint against rivets for the same thickness and geometry of connected elements. Moreover, the failure mode in the case of STS connectors is more ductile in contrast to the brittle failure of rivets. Another significant advantage of STS connectors, considering the recycle/reuse paradigm in a sustainability context, is that it allows the disassembling of elements and their reuse in different configurations.

The thickness of the steel sheet has a significant influence on the overall behavior of joints, in contempt of the connector type. The experimental results determined the average load-displacement curves. These curves highlighted that the highest load-carrying capacity occurred for the B series (thicker steel sheet). The connector type played a secondary role in the carrying capacity; the STS connectors yield higher applied force values than the SSPR connectors. The latter resulted in a 60% drop in the ultimate load values concerning the SRS connector for both the A and B series of samples. Moreover, the SRS joint failure occurred gradually and was more ductile than the brittle behavior of SSPR joints.

The presence of drawn-cups leads to a 10% increase in the initial stiffness of the joints and facilitates an easier alignment of the pre-drilled CFS profiles to be connected.

The FEA models of the tested joints using linear elements ran in two ways: considering the conventional hinged joints between the elements and hinged joints with axial stiffness based on either bilinear or polynomial definition of the P-Δ curve. The paper presents both linear and non-linear static analyses. The FE model using the polynomial behavior of the hinge leads to obtaining the closest results to the experiments being 12–15% more flexible than the manufactured joints. The presence of drawings, not considered in the numerical model, can explain this slight difference.

The calibrated model was used in a case study of a truss element frequently used in the flooring systems. Further investigating the obtained results and running a comparative analysis on the reported data from the scientific literature lead to the conclusion that the use of linear static analysis may produce erroneous results because there is a tendency of underestimating the structural response.

There are a currently growing number of scientific papers using complex numerical models and proposing joining solutions using self-tapping screws and/or rivets to improve the overall behavior of CFS elements and sub-systems. However, their applicability in practical design and construction processes is not an easy process. Moreover, the currently available design regulation, e.g., Eurocode 3, covers partly only the checking of the CFS elements joints, mainly in terms of strength, somehow neglecting the influence of joint stiffness. The present study did not focus on checking the strength requirement for T-joints but mainly on joint behavior influence regarding stiffness and connector type.

Although the strength requirement was fulfilled, with the maximum normal stress values being well below the strength of the steel sheet or the screw strength, the truss element considered for the case study proved to be quite flexible. The maximum intensity of the applied load that could produce normal stress equal to 98% of the material strength has given rise to a maximum vertical displacement of 100 mm, five times larger than the allowable limit. Consequently, such elements should also be checked concerning stiffness requirement, not only regarding strength. Additionally, the numerical models should account for the non-linear behavior of the joints based on laboratory tests since the classical approach of perfect hinged elements does not reflect the authentic truss system behavior.

7. Conclusions

The sustainability of civil engineering structures can and should matter from the early design stages. That is probable to turn up through an optimum design in terms of chosen construction materials coupled with a realistic behavior of structural elements in numerical models. That ensures the best use of employed materials and, at the same time, the degree of safety required by norms.

Cold-formed steel profiles are a promising alternative to their hot-rolled counterparts, especially when considering their beneficial load-carrying capacity to material consumption ratio. Another significant advantage of their recycling/reuse approach is the ability to be reused in different configurations, especially when STS connectors are in use.

The paper presents the experimental and numerical investigation of two types of connectors frequently used in the construction industry for manufacturing joints made of CFS profiles: steel-steel pop-rivets (SSPR) and self-tapping screws (STS). The experiments carried out in the case of T-joints subjected to tensile forces tested both solutions. The recorded videos of the experiments are available online [50,51]. Another significant parameter of the research was the thickness of the steel sheet used to make the CFS profiles.

The goal of the experimental program was to obtain valuable information on T-joint behavior in terms of strength and stiffness and to render evidence on failure mechanisms considering the connector type and thickness of CFS profiles.

A case study was considered for which the obtained load-displacement curves for the T-joints were used in the modeling of a truss structure by means of 1D finite elements and the behavior of hinges derived from the experimental program. The numerical models considered three distinct approaches in terms of hinge behavior: classical linear elastic analysis and two non-linear analysis cases. The non-linear cases considered bilinear and polynomial load-displacement curves for hinges based on experimentally obtained data.

Based on the obtained results from the FEA, it can be concluded that the linear model with infinite axial stiffness and only rotational degree free yields result that do not match the real behavior of the T-joint, whereas out of the two non-linear cases, the polynomial approach leads to the most accurate prediction of the authentic behavior.

The outcomes have a significant impact on the design stage of CFS elements. Although Eurocode 3 provides information on the design steps of CFS members connected using either SSPR or STS, it recommends taking in account the P-Δ effect for the influence of the joint stiffness on the overall behavior of the structural sub-systems. The investigated case study of the truss structure by the calibrated numerical model of the joints reveals the fact that for similar intensities of the applied load, the corresponding vertical displacement is 20 times lower for the case of linear static analysis based on classical hinged joints with

infinite axial stiffness compared to the non-linear approach accounting for the joint stiffness experimentally uniaxial determined.

The main conclusion of the research presented in this paper is that the design process should be as accurate as possible and account for all phenomena occurring either at the joints or within the elements themselves to obtain safe and sustainable structures using CFS elements. The numerical models, calibrated using experimental data, may lead to accurate results for overall structural rigidity, and may also have a significant influence on fulfilling strength requirements.

Presented outcomes should further progress to provide statistically relevant interpretations summarized in the form of load-displacement curves defining the behavior of different joint geometries using various types of connectors. Moreover, supplementary tests on cyclic loading at tension and compression are necessary because the fatigue of the joint influences the behavior and the axial stiffness of the connected elements. Presented results could serve as a starting point for further research on the spatial structural system behavior subjected to static loads.

Author Contributions: Conceptualization, G.T. and V.-M.V.; methodology, G.T., V.-M.V. and I.O.-D.; software, G.T. and V.-M.V.; validation, I.O.-D., A.R. and I.-O.T.; formal analysis, G.T., V.-M.V.; investigation, G.T. and V.-M.V.; resources, V.-M.V.; data curation V.-M.V. and I.-O.T.; writing—original draft preparation, G.T. and I.O.-D.; writing—review and editing A.R. and I.-O.T.; visualization, G.T.; supervision, V.-M.V., I.-O.T. and A.R.; project administration, A.R.; funding acquisition, A.R. All authors have read and agreed to the published version of the manuscript.

Funding: The APC was funded by the Erasmus+ project KA2—Higher education strategic partnerships no.2018-1-RO01-KA203-049214, *Rehabilitation of the Built Environment in the Context of Smart City and Sustainable Development Concepts for Knowledge Transfer and Lifelong Learning*—RE-BUILT.

Institutional Review Board Statement: Not applicable.

Informed Consent Statement: Not applicable.

Data Availability Statement: Not applicable.

Acknowledgments: The authors would like to thank SC Panoterm SRL, Iasi, Romania for supplying the T-joints in the various configurations used in the research. Their interest and continuous support is greatly acknowledged.

Conflicts of Interest: The authors declare no conflict of interest.

References

1. Thirunavukkarasu, K.; Kanthasamy, E.; Gatheeshgar, P.; Poologanathan, K.; Rajanayagam, H.; Suntharalingam, T.; Dissanayake, M. Sustainable Performance of a Modular Building System Made of Built-Up Cold-Formed Steel Beams. *Buildings* **2021**, *11*, 460. [CrossRef]
2. Liang, H.; Roy, K.; Fang, Z.; Lim, J.B.P. A Critical Review on Optimization of Cold-Formed Steel Members for Better Structural and Thermal Performances. *Buildings* **2022**, *12*, 34. [CrossRef]
3. Schafer, B.W. Cold-Formed Steel Structures around the World. *Steel Constr.* **2011**, *4*, 141–149. [CrossRef]
4. Blandford, G.E.; Louis, S. *Current Research on Cold-Formed Steel Structures*; Missouri University of Science and Technology: Rolla, MO, USA, 1990.
5. Ungureanu, V.; Both, I.; Burcă, M.; Nguyen, T.H.; Grosan, M.; Dubină, D. Experimental Investigations on Spot Welded Built-Up Cold-Formed Steel Beams. *Bull. Polytech. Inst. Jassy Constr. Archit. Sect.* **2018**, *64*, 19–30. [CrossRef]
6. Koh, H.; Blum, H.B. A Review of Current Practice for Testing by Analysis of Cold-Formed Steel Structures. *Structures* **2022**, *37*, 871–880. [CrossRef]
7. Sani, M.S.H.M.; Muftah, F.; Osman, A.R. A Review and Development of Cold-Formed Steel Channel Columns with Oriented Strand Board Sections. *Mater. Today Proc.* **2019**, *17*, 1078–1085. [CrossRef]
8. Moga, L.; Petran, I.; Santos, P.; Ungureanu, V. Thermo-Energy Performance of Lightweight Steel Framed Constructions: A Case Study. *Buildings* **2022**, *12*, 321. [CrossRef]
9. Campiche, A.; Shakeel, S.; Macillo, V.; Terracciano, M.T.; Bucciero, B.; Pali, T.; Fiorino, L.; Landolfo, R. Seismic Behaviour of Sheathed CFS Buildings: Shake Table Tests and Numerical Modelling. *Ing. Sismica* **2018**, *35*, 106–123.
10. Terracciano, M.T.; Bucciero, B.; Pali, T.; Macillo, V.; Fiorino, L.; Landolfo, R. Shake Table Tests of Structures with CFS Strap-Braced Stud Walls. *Key Eng. Mater.* **2018**, *763*, 432–439. [CrossRef]

11. Macillo, V.; Fiorino, L.; Landolfo, R. Seismic Response of CFS Shear Walls Sheathed with Nailed Gypsum Panels: Experimental Tests. *Thin-Walled Struct.* **2017**, *120*, 161–171. [CrossRef]
12. Gălăţanu, T.F.; Ungureanu, V. *The Experimental Tests of the Joint Assembly of Thin Walled Steel Profiles KB*; Transilvania University Publishing House Braşov: Braşov, Romania, 2012.
13. Ungureanu, V.; Luka•ević, I.; Both, I.; Dubina, D. Numerical Investigations on Built-up Cold-formed Steel Beams for Long Spans. *Ce/Papers* **2021**, *4*, 2277–2284. [CrossRef]
14. Lukačević, I.; Ungureanu, V.; Valčić, A.; Ćurković, I. Numerical Study on Bending Resistance of Cold-formed Steel Back-to-back Built-up Elements. *Ce/Papers* **2021**, *4*, 487–494. [CrossRef]
15. Taranu, G.; Toma, I.O. Experimental Investigation and Numerical Simulation of C-Shape Thin-Walled Steel Profile Joints. *Buildings* **2021**, *11*, 636. [CrossRef]
16. Senkardesler, O.; Goler, G.; Soyoz, S. Dynamic and Cyclic Response of a Full-Scale 2-Storey Cold-Formed Steel Structure with and without Infill Materials. *Bull. Earthq. Eng.* **2017**, *15*, 3207–3226. [CrossRef]
17. Hui, C.; Gardner, L.; Nethercot, D.A. Moment Redistribution in Cold-Formed Steel Continuous Beams. *Thin-Walled Struct.* **2016**, *98*, 465–477. [CrossRef]
18. Kyvelou, P.; Gardner, L.; Nethercot, D.A. Composite Action between Cold-Formed Steel Beams and Wood-Based Floorboards. *Int. J. Struct. Stab. Dyn.* **2015**, *15*, 1540029. [CrossRef]
19. Kyprianou, C.; Kyvelou, P.; Gardner, L.; Nethercot, D.A. Characterisation of Material and Connection Behaviour in Sheathed Cold-Formed Steel Wall Systems—Part 2: Analytical Modelling. *Structures* **2021**, *30*, 1184–1199. [CrossRef]
20. Liu, P.; Peterman, K.D.; Yu, C.; Schafer, B.W. Characterization of Cold-Formed Steel Shear Wall Behavior under Cyclic Loading for the CFS-NEES Building. In *Proceedings of the 21st International Specialty Conference on Cold-Formed Steel Structures—Recent Research and Developments in Cold-Formed Steel Design and Construction*; Missouri University of Science and Technology: Rolla, MO, USA, 2012.
21. Foroughi, H.; Wei, G.; Torabian, S.; Eatherton, M.R.; Schafer, B.W. *Seismic Behavior of Steel SCBF Buildings Including Consideration of Diaphragm Inelasticity*; Cold-Formed Steel Research Consortium Report Series; Johns Hopkins University: Baltimore, MD, USA, 2021.
22. Singh, A.; Wang, X.; Torabian, S.; Hutchinson, T.C.; Peterman, K.D.; Schafer, B.W. Seismic Performance of Symmetric Unfinished CFS In-Line Wall Systems. In *Structures Congress 2020*; American Society of Civil Engineers: Reston, VA, USA, 2020.
23. Xu, Y.; Zhou, X.; Shi, Y.; Zou, Y.; Xu, L.; Xiang, Y.; Ke, K. Lateral Resistance of OSB Sheathed Cold-Formed Steel Shear Walls. *Thin-Walled Struct.* **2021**, *161*, 107451. [CrossRef]
24. Wang, C.; Yang, Z.; Zhang, Z.; Qi, R. Experimental Study on Shear Behavior of Cold-Formed Steel Shear Walls with Bracket. *Structures* **2021**, *32*, 448–460. [CrossRef]
25. Zhao, J.; Peng, Y.; Su, W.; Dong, J. Finite Element Analysis of the Shear Capacity of Stainless-Steel Blind-Rivet Connections. *J. Constr. Steel Res.* **2021**, *179*, 106558. [CrossRef]
26. Roy, K.; Lau, H.H.; Ting, T.C.H.; Chen, B.; Lim, J.B.P. Flexural Capacity of Gapped Built-up Cold-Formed Steel Channel Sections Including Web Stiffeners. *J. Constr. Steel Res.* **2020**, *172*, 106154. [CrossRef]
27. Chen, B.; Roy, K.; Fang, Z.; Uzzaman, A.; Raftery, G.; Lim, J.B.P. Moment Capacity of Back-to-Back Cold-Formed Steel Channels with Edge-Stiffened Holes, Un-Stiffened Holes, and Plain Webs. *Eng. Struct.* **2021**, *235*, 112042. [CrossRef]
28. Dar, M.A.; Subramanian, N.; Rather, A.I.; Dar, A.R.; Lim, J.B.P.; Anbarasu, M.; Roy, K.; Dar, M.A.; Subramanian, N.; Rather, A.I.; et al. Effect of Angle Stiffeners on the Flexural Strength and Stiffness of Cold-Formed Steel Beams. *Steel Compos. Struct.* **2019**, *33*, 225. [CrossRef]
29. SFIA-Steel Framing Industry Association. Available online: https://sfia.memberclicks.net/sustainable-steel (accessed on 23 February 2022).
30. Maribeth Rizzuto Building with Sustainable Green Materials. Available online: https://www.buildings.com/articles/32274/building-sustainable-green-materials (accessed on 23 February 2022).
31. Jaspart, J.-P.; Weynand, K. *Design of Joints in Steel and Composite Structures*; ECCS–European Convention for Constructional Steelwork: Brussels, Belgium, 2016; ISBN 9789291471324.
32. Ye, J.; Jiang, L. Simplified Analytical Model and Shaking Table Test Validation for Seismic Analysis of Mid-Rise Cold-Formed Steel Composite Shear Wall Building. *Sustainability* **2018**, *10*, 3188. [CrossRef]
33. Lee, Y.H.; Tan, C.S.; Mohammad, S.; Md Tahir, M.; Shek, P.N. Review on Cold-Formed Steel Connections. *Sci. World J.* **2014**, *2014*, 951216. [CrossRef]
34. Tunca, O.; Erdal, F.; Sağsöz, A.E.; Çarbaş, S. Structural Features of Cold-Formed Steel Profiles. *Chall. J. Struct. Mech.* **2018**, *4*, 77. [CrossRef]
35. Pekoz, T.; Louis, S. *Design of Cold-Formed Steel Screw Connections*; Missouri University of Science and Technology: Rolla, MO, USA, 1990; pp. 575–579.
36. Flodr, J.; Lehner, P.; Krejsa, M. Experimental and Numerical Evaluation of Clinch Connections of Thin-Walled Building Structures. *Sustainability* **2020**, *12*, 5691. [CrossRef]
37. Huynh, M.T.; Pham, C.H.; Hancock, G.J. Design of Screwed Connections in Cold-Formed Steels in Shear. *Thin-Walled Struct.* **2020**, *154*, 106817. [CrossRef]

38. Alpatov, V.; Soloviev, A. Thin-Walled Profiles and Their Joint Assembly Units Built with Screws: Numerical Studies of Load Bearing Capacity. In Proceedings of the MATEC Web of Conferences, Wellington, New Zealand, 10–12 December 2018; EDP Sciences: Les Ulis, France; Volume 196.
39. Roy, K.; Lau, H.H.; Ting, T.C.H.; Masood, R.; Kumar, A.; Lim, J.B.P. Experiments and Finite Element Modelling of Screw Pattern of Self-Drilling Screw Connections for High Strength Cold-Formed Steel. *Thin-Walled Struct.* **2019**, *145*, 106393. [CrossRef]
40. Huynh, M.T.; Pham, C.H.; Hancock, G.J. Experimental Behaviour and Modelling of Screwed Connections of High Strength Sheet Steels in Shear. *Thin-Walled Struct.* **2020**, *146*, 106357. [CrossRef]
41. Kechidi, S.; Fratamico, D.C.; Bourahla, N.; Castro, J.M.; Schafer, B.W. Numerical Study of Screw Fasteners in Built-up CFS Chord Studs. *Ce/Papers* **2017**, *1*, 1543–1552. [CrossRef]
42. *EN 1993-1-1*; Eurocode 3: Design of Steel Structures—Part 1-1: General Rules and Rules for Buildings. CEN: Brussels, Belgium, 2005.
43. *EN 1993-1-3*; Eurocode 3: Design of Steel Structures—Part 1-3: General Rules, Supplementary Rules for Cold-Formed Thin Gauge Members and Sheeting. CEN: Brussels, Belgium, 2006.
44. *EN 1993-1-8*; Eurocode 3: Design of Steel Structures—Part 1-8: Design of Joints. CEN: Brussels, Belgium, 2005.
45. *EN 1993-1-5*; Eurocode 3: Design of Steel Structures—Part 1-5: Plated Structural Elements. CEN: Brussels, Belgium, 2006.
46. Kalo, R. High Fidelity Modeling of Cold-Formed Steel Single Lap Shear Screw Fastened Connections. Master's Thesis, University of Massachusetts Amherst, Amherst, MA, USA, 2019.
47. Rautenbach, E. Finite Element Modelling of Thin Sheet Steel Screw Connections. Master's Thesis, University of Pretoria, Pretoria, South Africa, 2016.
48. ROCAST—Catalog. Available online: https://vinix.cld.bz/ROCAST/html-Catalog-Rocast-2017-2018/125#zoom=z (accessed on 4 December 2021).
49. Robot Structural Analysis Professional. Available online: https://www.autodesk.com/products/robot-structural-analysis/overview (accessed on 13 January 2022).
50. S1 Pop-Rivets T-Joint Test of Thin-Walled Steel Profiles. Available online: https://youtu.be/3COo5riXSuk (accessed on 13 January 2022).
51. Self-Tapping Screw T-Joint Test. Available online: https://youtu.be/7zbe4oWyAmQ (accessed on 13 January 2022).